## Title
# Photodecay of guaiacol is faster in ice, and even more rapid on ice, than in aqueous solution.



## Journal
Environmental science. Processes & impacts, 22(8)

## ISSN
2050-7887

## Authors
Hullar, Ted
Bononi, Fernanda C
Chen, Zekun
et al.

## Publication Date
2020-08-01

## DOI
10.1039/d0em00242a

Peer reviewed

# Photodecay of guaiacol is faster in ice, and even more rapid on ice, than in aqueous solution

Ted Hullar[1], Fernanda Bononi[2], Zekun Chen[2], Danielle Magadia[1,3], Oliver Palmer[1,4], Theo Tran[1], Dario Rocca[5], Oliviero Andreussi[6], Davide Donadio[2], and Cort Anastasio[1,*]

[1] Department of Land, Air and Water Resources, University of California, Davis, One Shields Avenue, Davis, CA 95616, USA

[2] Department of Chemistry, University of California, Davis, One Shields Avenue, Davis, CA 95616, USA

[3] Now at California Air Resources Board, 1001 I Street, Sacramento, CA 95814

[4] Now at TeraPore Technologies, 407 Cabot Road, South San Francisco, CA 94080

[5] Université de Lorraine, CNRS, LPCT, F-54000 Nancy, France

[6] Department of Physics, University of North Texas, 1155 Union Circle, #311427, Denton, Texas 76203.

[*] Corresponding author, canastasio@ucdavis.edu, (530) 754-6095

## Environmental Significance Statement

Snow has long been recognized as an important part of our environment, providing benefits ranging from transportation to drinking water. More recently, research has revealed snow to be a particularly important site for photochemical reactions, for reasons including deep penetration of light into the snowpack and long summer days in polar regions. However, there is considerable debate over the speed of these reactions, with some research showing faster photodegradation of chemicals on snow or ice versus aqueous solution. Using guaiacol as a model compound, we found reaction rates at the snow surface were considerably faster than in solution, primarily due to increased quantum yield. These results indicate some chemicals in/on snow degrade faster than previously known, reducing their environmental lifetimes.

## Abstract

Snowpacks contain a wide variety of inorganic and organic compounds, including some that absorb sunlight and undergo direct photoreactions. How the rates of these reactions in, and on, ice compare to rates in water is unclear: some studies report similar rates, while others find faster rates in/on ice. Further complicating our understanding, there is conflicting evidence whether chemicals react more quickly at the air-ice interface compared to in liquid-like regions (LLRs) within the ice. To address these questions, we measured the photodegradation rate of guaiacol (2-methoxyphenol) in various sample types, including in solution, in ice, and at the air-ice interface of nature-identical snow. Compared to aqueous solution, we find modest rate constant enhancements (increases of 3- to 6-fold) in ice LLRs, and much larger enhancements (of 17- to

77-fold) at the air-ice interface of nature-identical snow. Our computational modeling suggests the absorption spectrum for guaiacol red-shifts and increases on ice surfaces, leading to more light absorption, but these changes explain only a small portion (roughly 2 to 9%) of the observed rate constant enhancements in/on ice. This indicates that increases in the quantum yield are primarily responsible for the increased photoreactivity of guaiacol on ice; relative to solution, our results suggest that the quantum yield is larger by a factor of roughly 3-6 in liquid-like regions and 12-40 at the air-ice interface.

## 1.0 Introduction

Snow is an active location for chemical reactions,[1,2] which can release pollutants to the atmosphere, act as sinks for toxic species, and alter the concentrations of markers used in ice core research to understand past atmospheres.[3] For example, photochemical reactions of organic compounds – some of which are toxic – transform the pollutants into more volatile molecules, such as formaldehyde, that can be released to the atmosphere.[4,5]

Deposited snow and ice are primarily composed of crystalline water ice, but also contain small areas of disordered water molecules where most solutes reside.[1,3,6,7] These disordered regions exist both at the air-ice interface (which is also referred to as the quasi-liquid layer (QLL) or disordered interface) and within liquid-like regions (LLRs) in the ice matrix (e.g., at grain boundaries). Much of snowpack chemistry appears to be driven by light,[3] in part because sunlight can reach tens of centimeters into the snowpack.[8-10] Compounds that absorb sunlight can undergo direct photoreactions, i.e., chemical transformations as a result of the absorbed energy.

Despite their importance, the rates of relatively few direct photochemical reactions in snow and ice have been quantified. Further confounding our understanding, past results give conflicting pictures of reaction rates for molecules in/on ice, with some work showing rate enhancements in/on ice compared to solution and other work showing no enhancement. Early work by Kahan and Donaldson [11] found that rates of photodegradation for toxic polycyclic aromatic hydrocarbons (PAHs) were enhanced on ice compared to in aqueous solution. For example, anthracene and naphthalene photodegradations were approximately six and nine times faster, respectively, at the air-ice interface. Later work from the same group[12] found a four-fold rate enhancement for anthracene at the interface and only a 1.6-fold enhancement in LLRs. Photodegradation of the aromatic compound harmine at the air-ice interface was enhanced by a factor of 4 compared to solution, but was not measured in LLRs.[13]

In contrast to these studies showing rate enhancements in/on ice, other work has found that photodegradation is not enhanced in ice relative to solution. For example, direct photodegradation of a number of inorganic solutes, including nitrate, nitrite, and hydrogen peroxide, is described by the same temperature-dependent relationship in LLRs and in aqueous solution.[14-16] In addition, similar rates in solution and ice LLRs have been reported for phenanthrene, pyrene, and fluoranthene.[17] Similarly, we found that anthracene and pyrene each had similar photodegradation rates in solution, in ice LLRs, and at the air-ice interface.[18]

The rate of photodecay for chemical "C" (M $s^{-1}$) in a low-light absorbing medium (e.g., solution or ice) during sunlight illumination is:[16]

$$\frac{d[C]}{dt} = -\sum_{\lambda} \frac{2303}{N_A} I_{\lambda}\, \Delta\lambda\, \Phi_{C,\lambda}\, \varepsilon_{C,\lambda}\ [C] \qquad (1)$$

where 2303 is a factor for units and base conversion (1000 $cm^3$ $L^{-1}$), $N_A$ is Avogadro's number (6.022 × $10^{23}$ molecules $mol^{-1}$), $I_{\lambda}$ is the actinic flux at each wavelength (photons $cm^{-2}$ $s^{-1}$ $nm^{-1}$), $\Delta\lambda$ is the wavelength interval between photon flux data points (nm), $\varepsilon_{C,\lambda}$ is the wavelength-dependent molar absorptivity for C ($M^{-1}$ $cm^{-1}$), $\Phi_{C,\lambda}$ is the quantum yield for loss of C (molecule $photon^{-1}$), and [C] is the concentration. Based on equation 1, three factors could enhance reaction rates in/on ice relative to solution: higher local photon fluxes, higher quantum yields, and/or a bathochromic shift (i.e., to longer wavelengths) in molar absorptivity, which shifts light absorption to regions with more photons.

Most previous work did not measure photon fluxes, making it difficult to fully assess whether the photon flux might have been higher in/on ice compared to solution. While the photon flux in near-surface snow can be up to twice as high as in the overlying air,[8,19,20] enhancements in laboratory ices are smaller.[21] Thus, differences in photon fluxes between ice and solution do not appear to be able to explain the observed ice enhancements in past work.

The second possibility is an enhancement in the quantum yield for loss, i.e., the fraction of absorbed photons that results in loss of C. Quantum yields for PAHs are similar in LLRs and solution,[17] while quantum yields for nitrate, nitrite, and hydrogen peroxide in LLRs follow the same temperature dependence as in aqueous solution, suggesting similar reaction environments.[14-16] However, Zhu and coworkers[22] reported a quantum yield for nitrate photolysis at the air-ice interface that is over 200 times higher than found by Chu and Anastasio[16] for nitrate in LLRs. Further, McFall et al.[23] recently found that nitrate photolysis is more efficient at the air-ice interface compared to in LLRs, but only by a factor of ~ 3. However, even at this lower enhancement, a higher quantum yield could explain a significant portion of the reported reaction rate increases for PAHs at the air-ice interface.

The third possible reason for an enhancement in rates of direct photodegradation in/on ice is that the molar absorptivities are shifted to the red (i.e., bathochromically). Because the abundance of solar photons increases dramatically at longer wavelengths between 290 and 400 nm, even a small bathochromic shift of absorbance in/on ice could significantly increase the rate of sunlight absorption and thus the reaction rate. Several studies have examined this possibility by measuring absorbance in LLRs and/or at the air-ice interface for a variety of chemicals.[24-30] For phenols and naphthalene, absorbance in/on ice is the same as in aqueous solution,[26,28] while anisole exhibits a small 4-nm bathochromic (red) shift in both LLRs and QLLs relative to solution.[29] Three aniline derivatives show a substantial 10-15 nm red shift in both LLRs and QLLs.[30] In contrast, methylene blue, nitrate, and nitrite in LLRs exhibit hypsochromic (blue) shifts of approximately, 10, 1, and 2 nm, respectively.[27] However, measuring absorbance at the air-ice interface can be problematic because it requires a relatively high concentration of molecules, which tends to lead to self-association, possibly changing absorption relative to what occurs for the much lower concentrations in natural snow.

Because of the difficulties in experimentally measuring light absorbance of molecules at the air-ice interface, a number of groups have instead relied upon molecular modeling.[31-34] In particular, quantum chemical (QC) calculations have been used to interpret spectroscopic measurements of UV-Vis absorption and emission for organic compounds present in LLRs or at the air-ice interface.[25,28,29,35] However, the modeling approach used in these former works cannot directly predict shifts in the UV-visible spectra due to different solvation environments.

Previous experimental work done with solutes on ice surfaces, in our laboratory and others, have attempted to reproduce the physical reaction environment of snow by a variety of methods, including freezing aqueous solution in molds, spraying aqueous solutions into liquid nitrogen to form ice pellets, or grinding solute-containing ices into small pieces.[8,12,15,16,36,37] However, snow crystals are quite complex, and none of these past methods for making impurity-containing snow analogs accurately mimic the complex structure and measured physical properties of newly-fallen natural snow crystals. For example, new natural snow has a specific surface area (SSA, the ratio of sample surface area to ice mass) of approximately 1,000 $cm^2 g^{-1}$.[38] However, a frozen water sample in a beaker can have an SSA of <1 $cm^2 g^{-1}$, increasing the likelihood that a test compound vapor deposited to that ice surface will aggregate.

To address the relative importance of changes in quantum yield and/or absorbance in ice compared to solution, here we measure the photodegradation rate constant of a model organic compound, guaiacol, which is emitted from biomass burning.[39] We study guaiacol (GUA) photodecay in several experimental preparations, including in solution, in ice, and at the air-ice interface on nature-identical snow crystals. In each case we measure photon fluxes to account for this variable. We also use a multiscale approach,[40] based on molecular dynamics (MD), quantum-mechanical calculations and statistical learning, to model the absorbance of guaiacol in aqueous solution and on an ice surface. We have two main goals: 1) to examine whether direct photodegradation of guaiacol is enhanced either in LLRs or at the air-ice interface of nature-identical snow, relative to solution, and 2) to understand the mechanism(s) for any enhancements.

## 2 Methods

### 2.1 Materials

Guaiacol (98%) was from Sigma or TCI. Acetonitrile (HPLC grade) was from Acros. 2-nitrobenzaldehyde (2NB, 98%) was from Sigma-Aldrich. High purity water (MQ) was from house-treated R/O water that was run through a Barnstead International DO813 activated carbon cartridge and then a Millipore Milli-Q system ($\geq$ 18.2 MΩ cm).

### 2.2 Sample preparation

Most samples were illuminated in either a 5-ml glass beaker (made by cutting the threads and neck off a 7-ml glass vial) or 10-ml glass beaker (Pyrex). Samples were covered with polyethylene film (ClingWrap brand, Glad Products Company, approximately 8 μm thick), held in place with an o-ring, to control guaiacol evaporation and sample contamination.

Samples were prepared with one of five different methods (Supplementary Figure S1): 1) Aqueous solution, where guaiacol was dissolved in MQ water to give a final concentration of 1.0 μM, then either 5 or 10 ml of solution was placed in a beaker and covered. 2) Freezer frozen solution, where 5 or 10 ml of a 1.0 μM aqueous solution was placed in a beaker, covered, and frozen in a laboratory freezer at -20 °C over approximately 3 hours. 3) Liquid nitrogen frozen solution, where samples were prepared from aqueous solution, put into a beaker, then placed in a pan filled with liquid nitrogen to a depth of approximately 2 cm. Freezing took approximately 90 seconds. 4) Vapor deposition of gas-phase guaiacol to the top surface of frozen water ice; our method here follows the same approach as previously described.[18] First, 10 ml of MQ water was placed in a beaker, covered with PE film, and frozen in a laboratory freezer at -20 °C. Once frozen, samples were removed and uncovered, and a nitrogen stream containing gas-phase guaiacol was directed at the ice surface for 15 s. Samples were then covered and placed back in a laboratory freezer. 5) Vapor deposited to nature-identical snow. First, we made nature-identical snow crystals, using a custom-built machine based on previous work,[38,41,42] described in Supplementary Section S3 and shown in Figure S2. This device, which is placed in a cold room at approximately -15 °C, uses the principle of nucleating supersaturated water vapor to form snow crystals (Figures S3 and S4, and Supplemental Movie M1). To treat the snow with guaiacol, nitrogen from a tank in the cold room was directed first through a HDPE wide-mouth bottle (500 or 1000 ml) holding laboratory-made snow to introduce water vapor. The gas was then passed through a glass container holding 0.4 g of guaiacol solid and then through another 500- or 1000-ml HDPE bottle holding snow, where guaiacol was deposited to the snow. Supplementary Figure S1b shows the treatment system. The treated snow was then gently mixed using two stainless steel spoons and transferred to individual 5- or 10-ml beakers for subsequent illumination. In the case of the LC2 condition (described below), the snow was tamped down 10 mm with a plastic plug before covering so that the snow level was no higher than the level of the cooled aluminum block in the illumination system. We noticed some subsidence in the snow level, particularly at the center of the beaker for longer experiments, probably attributable to metamorphism in the snow crystals. However, the overall appearance of the snow did not change, and there was no evidence of melting.

### 2.3 Sample illumination, actinometry, and chemical analysis

Sample illumination generally followed the method described for anthracene and pyrene.[18] Sample beakers were set upright in a drilled aluminum holder to maximize heat transfer and minimize the impact of sample heating from the illumination source. Dark samples were covered with aluminum foil and placed in the illumination chamber along with illuminated samples. Sample temperatures were held at 5 (for aqueous) or -10 °C (for ice and snow). For all experiments, the light source was a filtered 1000 W Xenon arc lamp. The first set of experiments was done using an AM1.5 airmass filter (Sciencetech), intended to filter the lamp source to approximate solar sunlight. We identify these experiments as Light Condition 1 ("LC1"). However, we later determined this filter significantly transmits light between 250 and 290 nm, which does not exist in tropospheric sunlight. Therefore, we ran additional experiments with three optical filters to better simulate sunlight: the airmass filter, a 295 longpass filter to eliminate shorter wavelengths transmitted by the airmass filter, and a 400 shortpass filter (both from Andover Corporation) to eliminate longer wavelengths that contribute to sample heating; we refer to these experiments as being conducted under Light Condition 2 ("LC2").

After illumination, we melted the frozen samples and measured guaiacol concentrations using a Shimadzu HPLC [18] with an eluent of 60:40 acetonitrile:MQ water, a flow rate of 0.700 ml $min^{-1}$, and a detection wavelength of 276 nm. Frozen samples were melted (still covered with PE) and then transferred to HPLC autosampler vials for analysis.

We used 2-nitrobenzaldehyde (2NB) as a chemical actinometer to normalize for differing photon fluxes across sample types and experimental days.[18,20] With the exception of snow samples, on each experiment day we prepared actinometry samples with 10 μM 2NB using the same sample preparation and experimental treatment as in the parallel guaiacol illuminations, and illuminated the 2NB samples to measure $j_{2NB}$.[18] Because measuring $j_{2NB}$ in snow on each experimental day was not practical, we measured $j_{2NB}$ in snow and in aqueous solution on three different days, then calculated the ratio of snow to aqueous measurements. For subsequent guaiacol photodegradation experiments in snow, we used this ratio (0.38 ± 0.015 (1 SD) for 10-ml beakers, 0.36 ± 0.13 for 5-ml beakers) along with the measured aqueous $j_{2NB}$ on that day to estimate the snow $j_{2NB}$.

### 2.4 Determining rate constants and quantum yields for guaiacol loss

To determine guaiacol photodegradation rate constants we followed the same approach used by Hullar et al.[18] for PAHs. We illuminated samples, and periodically removed them from the illumination system and analyzed for guaiacol (section 2.3). For each experiment, we determined the photodegradation rate constant by first taking the natural logarithm of the ratio of each measured guaiacol concentration at time *t* to the initial guaiacol concentration, then adjusting these ratios by the photon-flux correction factor for each sample position.[18] The slope of these points gives the pseudo-first-order rate constant for loss during illumination, $j_{GUA}$. Similar treatment of the dark controls gives the rate constant for dark loss, $k'_{GUA,dark}$; subtracting the dark rate constant from $j_{GUA}$ gives the dark-corrected photodegradation rate constant, $j_{GUA,exp}$. Finally, to normalize for the experimental photon flux, we divided $j_{GUA,exp}$ by the daily measured $j_{2NB}$ value to give the photon flux-normalized $j^*_{GUA}$.

To calculate the average quantum yield for guaiacol ($\Phi_{GUA}$) we used our previously determined $j_{GUA,exp}$, which can be expressed as:

$$j_{GUA,exp} = \frac{2303}{N_A}\,\Phi_{GUA}\sum_{\lambda}(\varepsilon_{GUA,\lambda}\ I_{\lambda}\ \Delta\lambda) \qquad (2)$$

and solved this equation for $\Phi_{GUA}$. We determined molar absorptivities for guaiacol ($\varepsilon_{GUA,\lambda}$) by measuring absorbance spectra in five aqueous guaiacol solutions (10-1000 μM) at 25 °C using a UV-2501PC spectrophotometer (Shimadzu) in 1.0 cm cuvettes against a MQ reference cell. For each wavelength, we calculated the base-10 molar absorptivity as the slope of the linear regression of measured absorbance (divided by the 1-cm pathlength) versus the guaiacol concentration. As described in Supplementary Section S1, we determined $I_{\lambda}$ by measuring $j_{2NB}$ and relative photon fluxes at a reference position for each light condition. The quantum yield determined using equation 2 represents an average value over the guaiacol absorbance range of 250 to the end of absorption, approximately 317 nm.

### 2.5 Computational methods

We use a combination of classical and first-principles molecular dynamics (FPMD) simulations, excited state calculations by time-dependent density functional theory (TDDFT), and machine learning to determine UV-visible absorption bands at finite temperature, including the effects of both long-range and local dielectric screening. We performed first-principles MD simulations of guaiacol in solution at 27 °C and the air-ice interface at -10 °C, selected to represent experiments conducted in aqueous solution or at the air-ice interface, respectively. For the air-ice interface case, we used an ice slab model, with a well-equilibrated surface structure, in accordance with recent measurements of the quasi-liquid layer of ice.[43,44]

From each 50 ps-long MD simulation trajectory we extracted ~200 statistically independent frames, removed the explicit solvent molecules, and computed the absorption spectra using TDDFT.[45,46] To account for the screening effect of the solvent, we used a self-consistent continuous solvent (SCCS) model,[47,48] with a position-dependent dielectric permittivity of the environment. This newly developed feature allows one to treat molecules adsorbed at the interface between regions with different dielectric response, such as the air-ice interface. The ensemble average accounts for the configurational sampling at finite temperature in the specific solvation environment.[40,49]

To quantify the effect of the bathochromic shift on the molecular photodissociation rates, we refined the line shape of the lowest energy absorption band using a simple machine learning approach based on the least absolute shrinkage and selection operator (LASSO) regression model.[50] We verified that the TDDFT datasets obtained for guaiacol in solution and at the air-ice interface are suitable to train a single model, which we applied to 5000 frames from each FPMD trajectory. The LASSO model allows us to attain a finer estimate of the low-energy tails of the spectra, which is needed to calculate the rate of photon absorption for a given illumination condition. Additional details about the computational procedures and parameters are provided in Supplementary Information Section S2. The detailed implementation and validation of our multi-scale multi-model approach to calculate the shifts of UV-visible absorption spectra at the air-ice interface are described in depth in a separate manuscript.[51]

## 3 Results and Discussion

### 3.1 Example illumination experiment

Figure 1 shows a typical illumination experiment, with each point representing one snow-filled beaker. Dark controls show slight loss of guaiacol , most likely explained by volatilization, with a measured rate constant ($k'_{GUA,dark}$ ± 1 SE) of 0.00076 ± 0.00033 min$^{-1}$ ($R^2$ = 0.57). In the illuminated samples, we see much more loss due to photodegradation, with a rate constant ($j_{GUA}$ ± 1 SE) of 0.0033 ± 0.00032 s$^{-1}$ ($R^2$ = 0.91). Subtracting the dark loss from the light loss, and then dividing by the measured $j_{2NB}$ value for this experimental day (0.0024 s$^{-1}$), gives a normalized photodegradation rate ($j^*_{GUA}$ ± 1 SE) of 1.0 ± 0.19 min$^{-1}$/s$^{-1}$.

### 3.2 GUA photodegradation rate constants for each sample preparation method

As described in section 2.3, we illuminated our samples using two different light conditions. Figure 2 presents the results for experiments conducted under Light Condition 1 (LC1), where we unknowingly had significant a photon flux below 290 nm. We normalized the (dark-corrected) measured rate constants to the measured $j_{2NB}$ value for each experimental day to remove the impacts of differences in photon fluxes between different sample types. As shown in Figure 2, guaiacol photodegradation in aqueous solution occurs slowly, but is measurable and statistically greater than zero. Average normalized photodegradation rates constants ($j^*_{GUA}$) in freezer frozen and liquid nitrogen frozen samples are similar to each other, and approximately 3 times faster than in aqueous solution. For the next condition, where guaiacol was vapor-deposited to a water ice surface ("VD to ice surface"), the average $j^*_{GUA}$ is faster than in freezer frozen or liquid nitrogen frozen samples, but the data are highly variable and not statistically different from zero, making it difficult to draw any conclusions. Finally, for guaiacol vapor-deposited to nature-identical snow ("VD to snow") the average $j^*_{GUA}$ is similar to that for the vapor-deposited to ice surface samples. However, the experimental reproducibility is much better, and guaiacol in these samples clearly has a faster average $j^*_{GUA}$ than either the freezer frozen solution, liquid nitrogen frozen solution, or aqueous samples.

We used the Tukey-Kramer test for multiple comparisons ($P < 0.05$) to generate statistical groupings having statistically indistinguishable mean $j^*_{GUA}$ values, given by the letters A, B, and C across the top of Figure 2. Because of its high variability, the average $j^*_{GUA}$ for vapor-deposited to ice surface samples is indistinguishable from that of any of the other sample preparation method. Freezer frozen and liquid nitrogen frozen samples have means indistinguishable from each other. Each of the remaining sample types has differing $j^*_{GUA}$ values, with aqueous the lowest and vapor-deposited to snow the highest. As listed in Table 1, the ratio of $j^*_{GUA}$ for the aqueous : freezer frozen solution : liquid nitrogen frozen solution : vapor-deposited to snow results for LC1 is 1 : 2.6 : 3.3 : 17, with a typical propagated relative standard deviation of roughly 50% for each ratio.

To the best of our knowledge, our results are the first use of nature-identical snow to study photodegradation of a chemical at the air-ice interface. This technique has several clear advantages over vapor deposition to an ice surface. First, the much higher specific surface area reduces the likelihood of a test compound aggregating on the surface. Based on previous work with nature-identical snow made in a similar machine,[38] our snow likely has a specific surface area of around 600 $cm^2/cm^3$ (snow surface area/water volume). Assuming a single guaiacol molecule occupies a square 6 Å on a side and the molecules do not overlap, our maximum guaiacol concentration (9 μM) covers only 3% of the available snow surface. By contrast, the maximum guaiacol concentration in our vapor-deposited to ice samples (also 9 μM) would be approximately 60 molecules thick if distributed across a homogeneous ice surface in the illumination beaker. Secondly, the nature-identical snow findings are more representative of natural conditions, as most photodegradation taking place in snow-covered regions of the world occurs in snowpacks, not on monolithic ice surfaces. Finally, our experimental results show greater consistency on snow as opposed to ice surfaces, allowing more accurate determination of rate constants, as illustrated by the 95% CI error bars in Figure 2.

After completing illumination experiments using LC1, we discovered that our illumination system was passing significant amounts of light at wavelengths as low as 250 nm, whereas the lowest wavelength in polar tropospheric sunlight is approximately 290 nm. To remedy this problem and improve the experimental setup, we installed two additional optical filters in our system, a 295 longpass and a 400 shortpass: we term this Light Condition 2 (LC2). To reduce experimental variability and improve the statistical confidence of our results, we also tamped down LC2 snow samples approximately 10 mm and illuminated them for at least 24 hours. Figure 3 and Supplementary Figure S5 show the wavelength profiles for both LC1 and LC2, as well as the modeled actinic flux for solar noon on the summer solstice at Summit, Greenland. The 295 longpass filter significantly reduces wavelengths below 295 nm, while the 400 shortpass filter cuts out wavelengths from approximately 400 to 525 nm, which are irrelevant for guaiacol photodegradation but can heat and degrade frozen samples, particularly snow. Supplementary Figure S6 shows transmittance measurements for the three optical filters, as well as some other materials used in our experiments. While LC1 allowed considerable light emissions below 290 nm, LC2 does not, and is closer to the expected summer sunlight condition in a polar region such as Summit.

Using the LC2 condition, we reran illumination experiments for all illumination conditions except vapor-deposited to ice, with results shown in Figure 4 and Table 1. LC2 $j^*_{GUA}$ values are less than LC1 values because of two factors: first, there are fewer photons present at the wavelengths where guaiacol absorbs most strongly (250-290 nm, Figure 3), so $j_{GUA,exp}$ is considerably lower for LC2 and more similar to expected environmental values. Second, while 2NB absorbs more strongly at shorter wavelengths, it continues to absorb significant light up to 400 nm,[20] so measured $j_{2NB}$ values are only slightly less for LC2 than LC1 (Supplementary Tables S1 and S2). Despite being lower overall, $j^*_{GUA}$ values show the same relationship to each other under LC2 as LC1 (Table 1), with a ratio of aqueous : freezer frozen solution : liquid nitrogen frozen solution : vapor-deposited to snow of 1 : 6.3 : 5.4 : 77, and a relative standard deviation for each ratio of approximately 50%. Tukey-Kramer comparisons yield the same statistical groupings for LC2 as for LC1, shown by the letters A, B, and C on Figure 4: average $j^*_{GUA}$ values for freezer frozen solution and liquid nitrogen frozen solution sample treatments are statistically indistinguishable from each other, but statistically higher than aqueous, while the average $j^*_{GUA}$ value for guaiacol vapor deposited to snow is statistically higher than all other treatments. LC2 results support the same conclusions as LC1, that guaiacol at the air-ice interface has a considerably faster photodegradation rate constant than in aqueous solution and LLRs, and a somewhat faster photodegradation rate constant in LLRs than in aqueous solution. Interestingly, enhancement ratios relative to aqueous are higher for LC2 than LC1; because the guaiacol absorbance curve overlaps the LC2 photon flux curve less than the LC1 curve (Figure 3), experiments conducted using LC2 conditions may be more sensitive to a bathochromic shift in guaiacol absorbance, resulting in the higher ratios. The fact that the reactivity enhancement at the interface depends on the wavelength distribution of the photon fluxes highlights the importance of using good quality simulated sunlight in laboratory experiments.

While previous studies comparing photodegradation rate constants in aqueous solution, LLRs, and at the air-ice interface did not test guaiacol, several reported similar results as ours here, with rate constants somewhat faster in LLRs and considerably faster at the air-ice interface.[11-13]. However, the magnitude of the enhancements we found at the air-ice interface are significantly greater than have been reported before; while previous studies reported rate constant increases of 4- to 9-fold for organic compounds,[11-13] our results on ice range up to 77-fold. Taken together, these results suggest the photochemical reactivity for guaiacol is decidedly different at the air-ice interface, in LLRs, and in aqueous solution.

### 3.3 GUA photodegradation in samples with reduced dissolved oxygen

To confirm that guaiacol decay in our experiments is controlled by direct photochemistry and not indirect reactions with oxidants photoformed by trace contaminants, we examined the impact of removing dissolved oxygen for LC1 conditions. We were particularly concerned about oxidizing triplet excited states ($^3C^*$), which react readily with guaiacol and other phenols[52] and whose concentrations are enhanced by a factor of roughly 100 in ice LLRs relative to solution.[53] In an aqueous solution, dissolved oxygen is a major sink of $^3C^*$, so reducing the amount of $O_2$ should greatly increase the triplet steady-state concentration, with a resulting increase in the guaiacol degradation rate constant if $^3C^*$ were an important sink. We tested for this possibility by bubbling nitrogen (99.998% purity) at a flow rate of 40 ml $min^{-1}$ through 2 ml of 1 μM guaiacol aqueous solution in a 2-ml HPLC vial for 2 or 4 minutes, then capping with PTFE septum caps. We illuminated some samples as aqueous solution, and others after freezing in a laboratory freezer; both sample types were illuminated horizontally to avoid shading from the opaque caps.

As shown in Figure S7 and Table S3, deoxygenating made no statistically significant difference in guaiacol photodegradation in aqueous solution, indicating that direct photodegradation is the major sink. In frozen samples, the mean $j^*_{GUA}$ is roughly 40% lower in ice made from deoxygenated solution (compared to air-saturated solution), which is the opposite of what we would expect if $^3C^*$ were a major oxidant for guaiacol, indicating that triplets are insignificant oxidants. This small effect of deoxygenation suggests that trace oxygen-dependent oxidants (e.g., hydroxyl radical) could contribute to guaiacol loss during our ice illumination experiments, but indicates that the major sink for guaiacol in ice is direct photodegradation.

### 3.4 Light absorbance of guaiacol in solution and on at the air-ice interface

Our results in Figures 1 and 2 indicate that guaiacol photodegradation is significantly enhanced in ice, and especially on ice, compared to in solution. To understand the contribution of changes in guaiacol light absorption to this enhancement at the air-ice interface, we used multiscale molecular modeling to determine absorption at the interface. Figure 3 shows the measured absorption spectrum of guaiacol in solution (solid red line), along with measured photon fluxes for our two experimental conditions and TUV modelled values for Summit, Greenland in summer. The small overlap between the tail of the aqueous guaiacol absorption spectrum and the edge of the photon flux curves suggests that a red shift of the absorption band for guaiacol at the air-ice interface relative to aqueous solution would significantly enhance photodegradation. Figure 3 displays the lowest energy absorption bands for guaiacol in solution (dashed red line) and at the air-ice interface (dashed blue line), computed with our first-principles multiscale approach, with line-shapes refined using statistical learning. The theoretical spectra are normalized to the amplitude of the experimental absorption band. Considering that TDDFT tends to systematically underestimate excitation energies,[54] the agreement between the theory and experiment for guaiacol in solution is very good, as the difference between the measured and calculated peak positions is less than about 0.1 eV. Given the systematic nature of this shift,[49] differences computed for the same molecule in different environments (e.g., in solution and at the air-ice interface) are physically meaningful. Furthermore, the theoretical band is somewhat narrower than the experimental one, as it misses the tail of higher energy excitations, which are not taken into account in the machine-learning (ML) model. We used this ML model to refine the long-wavelength tail of the spectra, as this region is crucial to estimate the overlap between molar absorptivities and photon fluxes in different solvation conditions.

Supplementary Figure S9 shows that the ML model developed using the guaiacol molecule in both environments has a training $R^2$ of 0.863 and a testing $R^2$ of 0.815, along with a training mean absolute error (MAE) of 1.74 nm and a testing MAE of 1.99 nm. These statistical metrics suggest it is within reasonable accuracy (i.e. MAE ≤ 2nm) to use a single LASSO model, fitted on the space of a subset of molecular coordinates, to interpolate through the excitation energies of guaiacol both in aqueous solution and at the air-ice interface, and that the uncertainty of our calculated absorbance shift is approximately ± 2 nm. Further, the possibility to accurately fit the excitation energies to a single LASSO model indicates that the modeled bathochromic shift results from conformational changes to the guaiacol molecule caused by the local solvation environment (solution or air-ice interface), rather than dielectric differences in the solvation environment itself.

As shown in Figure 3, our modeling finds that the absorption spectrum of guaiacol at the air-ice interface undergoes two significant changes relative to that computed for guaiacol in solution: a bathochromic shift of ~5 nm and a small (6%) increase in intensity. A statistical analysis of the quantum-chemical excitation energies, computed from frames extracted from the FPMD trajectories, reveals that the guaiacol configuration is different on the ice surface compared to in solution, and indicates that the bathochromic shift (and intensity increase) is caused by such differences in the geometry of guaiacol , a model of which is shown in Figure 5a with heavy atoms and the OH group labeled from 1 to 10. Figure 5b shows the individual contribution of each atom to the absorbance spectrum difference in terms of the absolute magnitude of the weight parameters from the LASSO model ($|W_{LASSO}|$). This data shows that almost all of the absorbance shift can be evenly attributed to conformational changes of the six carbons in the guaiacol aromatic ring, with minor contributions from the other atoms. This in accordance with electronic structure calculations that show that both the HOMO and the LUMO states are localized on the phenyl group. The most important difference for the position of the lowest-energy absorption band amounts to an average change in the C-C bond length in the phenyl ring, i.e. the carbon atoms labeled 1-6 in Figure 5a. The average of these distributions, computed over ~5000 frames of each FPMD trajectory, is shifted by approximately 0.012 Å to longer distances for guaiacol on ice than in aqueous solution (Figure 5c). While other factors (such as bond angle) may also play a part, these results indicate geometric changes in the guaiacol aromatic ring are the major factor responsible for the change in light absorption at the air-ice interface.

### 3.5 Relative importance of changes in absorbance and quantum yields on photodegradation rates

Our guaiacol computational studies predict a bathochromic absorbance shift of approximately 5 nm on an ice surface relative to in aqueous solution, and a hyperchromic absorbance increase of approximately 6% (Figure 3). To assess the impact of these changes on guaiacol photodegradation rates, we first determined the rate constant for light absorbance in solution, i.e., the product of the molar absorptivity and photon flux (with some additional factors) at each wavelength, summed over all wavelengths (equation S6). We did this for our two experimental light conditions LC1 and LC2, as well as for the modeled summer Summit TUV actinic flux.[55] The area under each resulting curve gives the total rate constant of light absorption in solution for each illumination condition (Figure S8). To determine the rate constant of light absorption at the air-ice interface, we did the same procedure, but now with various changes (i.e., variable shifts and a 6% increase in absorption) in the aqueous absorbance spectrum to mimic absorbance on the ice surface. Assuming that the quantum yield for GUA loss is the same in solution and on ice, the ratio of rates of light absorption (with and without the changes) is equal to the ratio of the rate constants for guaiacol loss, i.e., $j^*_{GUA,shifted} / j^*_{GUA,no\ shift}$.

Figure 6 shows the impact of various red and blue shifts on the total rate constant of light absorption and, therefore, predicted $j^*_{GUA}$ values. Red-shifting the guaiacol absorbance spectrum moves the absorbance to wavelengths where there are more photons (Figure 3), increasing the rate constant of light absorption and the resulting rate constant for guaiacol photodegradation.

But for our laboratory light conditions the results are modest. For our best estimate of the red-shifting (5 nm) and hyperchromic absorbance increase (6%) that occurs with guaiacol on ice, the rate constant of light absorption relative to aqueous solution increases only by a factor of 1.5 (LC1) or 1.9 (LC2); incorporating our approximately 2-nm uncertainty in absorbance shift gives ranges of 1.3 - 1.6 and 1.5 - 2.4 for LC1 and LC2 respectively. In contrast, we measured photodegradation rate constant enhancements at the air-ice interface relative to aqueous solution of 17- and 77-fold for LC1 and LC2, respectively (Table 1). So changes in light absorption only explain a small portion (9% or less) of the observed enhancements in photodecay we measured for guaiacol at the air-ice interface. As we have controlled for photon fluxes in our experimental procedures, this suggests the remaining portion of the enhancement factors (11- to 13-fold for LC1 and 32- to 51-fold for LC2) is caused by an increase in the quantum yield for guaiacol photodegradation. In contrast to our laboratory photon flux results, the orange line in Figure 6 shows $j^*_{GUA,shifted} / j^*_{GUA,no\ shift}$ for various absorbance shifts using TUV-modeled actinic flux at Summit, Greenland. Because there is only slight overlap (at around 300 nm) between this polar actinic flux and the guaiacol absorbance curve (Figure 3), even small shifts in the absorbance spectrum cause large changes in the amount of light absorbed. For example, including the 6% absorbance increase and red-shifting the guaiacol spectrum by 1, 2, and 5 nm increases the rate constant for guaiacol photodecay by factors of 1.7, 2.7, and 11 respectively relative to aqueous solution, assuming no change in quantum yield.

Table 1 presents calculated quantum yields for guaiacol ($\Phi_{GUA}$) under our various experimental conditions. These are calculated using the aqueous guaiacol molar absorptivities for the solution, freezer frozen solution, and liquid nitrogen frozen solution conditions; for values at the air-ice interface (vapor-deposited to ice and vapor-deposited to snow), the calculations assume a 5-nm bathochromic absorbance shift and 6% increase in molar absorptivities relative to solution. Quantum yields are quite similar, nearly 3%, for aqueous solution in both LC1 and LC2 conditions. For preparations where guaiacol would largely be in LLRs (freezer frozen solution and liquid nitrogen frozen solution), quantum yields are roughly 8% in LC1 and 17% in LC2, 3 and 6 times greater than in aqueous solution, respectively. Because we did not model absorbance shifts in LLRs, it is possible that part of this apparent quantum yield increase could be attributable to small (< 5 nm) absorbance shifts in LLRs. It is also possible that these sample preparations place most of the guaiacol in LLRs, but also some at the air-ice interface, which would increase the apparent quantum yield.

Finally, Table 1 shows that calculated quantum yields (± 1 SD) at the air-ice interface of snow are very high – 31 (± 14) % for LC1 and 110 (± 50) % for LC2 – and are not statistically significantly different from each other ($P < 0.05$). These represent enhancements by factors of 12 and 40 compared to aqueous for the LC1 and LC2 conditions, respectively. The calculated quantum yield for LC2 snow encompasses the theoretical maximum of 1.0 mlc photon$^{-1}$, which is exceptionally – and possibly erroneously – high. It is possible that other, unaccounted, factors are contributing to this very high quantum yield. One possibility is that the true bathochromic shift for guaiacol at the air-ice interface is greater than the 5 nm predicted by our computational results, which would lower the calculated quantum yield. For example, a shift of 7 nm would reduce the LC2 vapor-deposited to snow quantum yield to 0.89 mlc photon$^{-1}$. Another possibility is that guaiacol is being lost via pathways other than direct photodegradation, including through photoformed oxidants. Our deoxygenation control tests of Section 3.3 suggest that oxidants are insignificant in aqueous solution but do play a role in guaiacol loss in ice. For this reason our quantum yields should be considered upper bounds.

## 4 Environmental implications and conclusions

Guaiacol is one of the many aromatic compounds emitted by biomass burning,[39] which is a significant source of organics to remote polar regions.[56-59] To understand what our experimental results mean for the lifetimes of guaiacol in polar snow, we calculated guaiacol photodegradation rate constants for Summit, Greenland under summer solstice sunlight. We used equation 1 with: the TUV modeled actinic flux at midday of the summer solstice; our estimated average $\Phi_{GUA}$ under LC2 for aqueous, LLRs (the average of freezer frozen solution and liquid nitrogen frozen solution values) and at the air-ice interface (vapor-deposited to snow); and our measured $\varepsilon_{GUA}$ (bathochromically shifted by 5 nm and increased by 6% for guaiacol at the air-ice interface). The resulting $j_{GUA}$ values for Summit summer sunlight are $1.2 \times 10^{-9}$, $7.0 \times 10^{-9}$, and $5.2 \times 10^{-7}$ $s^{-1}$ for aqueous solution, LLRs, and the air-ice interface, respectively, corresponding to photochemical lifetimes of 9,700, 1,600, and 22 days of midday summer solstice sunlight. In comparison, based on the typical concentration of hydroxyl radical (OH) in Summit snow ($2 \times 10^{-15}$ $M^{-1}$ $s^{-1}$; [60]) and the solution rate constant of OH with guaiacol (approximately $10^{10}$ $M^{-1}$ $s^{-1}$; [61]), the guaiacol lifetime with respect to OH oxidation in snow is roughly 14 hours. In addition, triplet excited states of brown carbon are likely a similarly important sink for guaiacol, as they react rapidly with phenols[52] and their concentrations are enhanced in ice.[53] These results indicate that while the photodecay of guaiacol at Summit is enhanced by a factor of roughly 100 at the air-ice interface compared to in LLRs, it is still relatively slow because of low light absorbance. In contrast, reaction with photooxidants is a much more important sink for guaiacol, rendering direct photoreaction unimportant. However, this is not a generalizable result, as the relative importance of oxidants and direct photoreaction will depend on the identity of the compound and its reactivity. To the best of our knowledge, reaction rates of guaiacol with oxidants such as the hydroxyl radical have not been studied in the various compartments found in snow, and further work is required in this area.

As best we know, this work represents the first time that nature-identical snow has been used to measure reaction rates at the air-ice interface. The major advantage of this approach is the very high specific surface area of the snow, which better mimics environmental conditions, reduces aggregation, and can provide more precise measurements than vapor deposition to an ice pellet. The computational methods used here provide realistic absorbance curves and allow estimation of absorbance shifts at the interface, which are difficult to measure. We found a statistically significant increase in photon-flux-normalized guaiacol photodegradation rate constants relative to aqueous solution for both LLRs and at the air-ice interface: the rate constant enhancement was modest for LLRs, ranging from 3- to 6-fold depending on the illumination conditions, but was larger at the air-ice interface, ranging from 10- to 77-fold. Computational modelling suggests approximately 2 - 9% of the rate constant increase we measure in the laboratory is attributable to a red-shift and increase of absorbance that occurs for guaiacol on the surface of ice compared to solution. This leads us to conclude the measured rate constant enhancements are largely due to increased quantum yields for guaiacol in frozen systems. The ratio of quantum yields for aqueous : LLRs : air-ice interface is 1 : 3 : 12 for our initial light condition (LC1) and 1 : 6 : 40 for LC2. In contrast, our calculations indicate that a shift in absorbance will have a more dramatic effect under polar sunlight; in the case of guaiacol on Summit snow, a 5-nm shift in absorbance combined with a 6% increase in molar absorptivities causes a 11-fold increase in the rate constant for light absorption, which is approximately equal to the factor of increase in quantum yield that occurs at the interface compared to LLRs.

Our computational finding here that the average guaiacol aromatic carbon-carbon bond length is approximately 1% longer on an ice surface than in aqueous solution, combined with the modeled 5 nm absorbance shift and 6% absorbance increase, suggests slight changes in atomic arrangements can produce significant alterations in molecular properties. As discussed earlier, previous work has shown faster photodegradation rate constants in LLRs or at the air-ice interface for some compounds, but not for others. Similarly, some studies have reported absorbance shifts (either red or blue) for compounds on ice surfaces, while others did not. Collectively, these results suggest properties such as bond length, absorbance, or quantum yield can be altered by the association between a molecule and an ice surface, but such changes are difficult to predict and may be compound specific. Additional work to evaluate chemical properties on ice surfaces, both experimental and computational, will be required to better understand ice-chemical interactions.

## Conflicts of Interest

There are no conflicts of interest to declare.


## Acknowledgments

We thank the National Science Foundation for funding (CHE 1806210 and AGS-PRF 1524857) and Rebecca Boulden and Raven Lyric for experimental assistance.

## Tables

**Table 1** Summary statistics for each experimental preparation method under Light Conditions 1 and 2[a]

| | Number of Experiments | $j^*_{GUA}$ [b] ($min^{-1}/s^{-1}$) | Enhancement[c] ($j^*_{GUA,\,i} / j^*_{GUA,\,aq}$) | Quantum Yield ($\Phi_{GUA}$)[d] (mlc $photon^{-1}$) |
|---|---|---|---|---|
| **LC1 (Light condition 1)** | | | | |
| Aqueous | 6 | 0.075 ± 0.012 | 1 | 0.027 ± 0.0045 |
| Freezer frozen solution | 6 | 0.20 ± 0.082 | 2.6 ± 1.2 | 0.07 ± 0.03 |
| Liquid nitrogen frozen solution | 4 | 0.25 ± 0.040 | 3.3 ± 0.8 | 0.089 ± 0.015 |
| Vapor-deposited to ice surface | 4 | 0.71 ± 0.52 | 9.5 ± 7.1 | 0.17 ± 0.13 |
| Vapor-deposited to snow | 6 | 1.28 ± 0.57 | 17 ± 8 | 0.31 ± 0.14 |
| **LC2 (Light condition 2)** | | | | |
| Aqueous | 3 | 0.0088 ± 0.0038 | 1 | 0.027 ± 0.012 |
| Freezer frozen solution | 3 | 0.056 ± 0.0063 | 6.3 ± 2.8 | 0.17 ± 0.021 |
| Liquid nitrogen frozen solution | 3 | 0.048 ± 0.0075 | 5.4 ± 2.5 | 0.15 ± 0.024 |
| Vapor-deposited to ice surface | 0 | | --- No experiments done --- | |
| Vapor-deposited to snow | 4 | 0.68 ± 0.26 | 77 ± 44 | 1.1 ± 0.5 |

[a] Samples were held at 5 °C (aqueous samples) or -10 °C (all other preparations).

[b] Listed $j^*_{GUA}$ values (photon-flux normalized photodegradation rate constants) are means ± 1 standard deviation.

[c] Enhancement factors are the ratio of the mean $j^*_{GUA}$ value for each preparation method to the mean aqueous $j^*_{GUA}$ value for that light condition, ± the propagated standard deviation.

[d] Quantum yields are calculated individually for each experiment from equation S7 in Supplementary Information Section S1, using the measured $j_{GUA,exp}$ and $j_{2NB}$. Uncertainties for quantum yields are the propagated standard deviation for $j_{GUA,exp}$ combined with the uncertainty for light absorption, assumed as 5% for aqueous, freezer frozen, and liquid nitrogen frozen sample types, or calculated from a 5 ± 2 nm absorbance shift for vapor-deposited samples (10% for LC1 or 25% for LC2 light conditions).

**Figures**

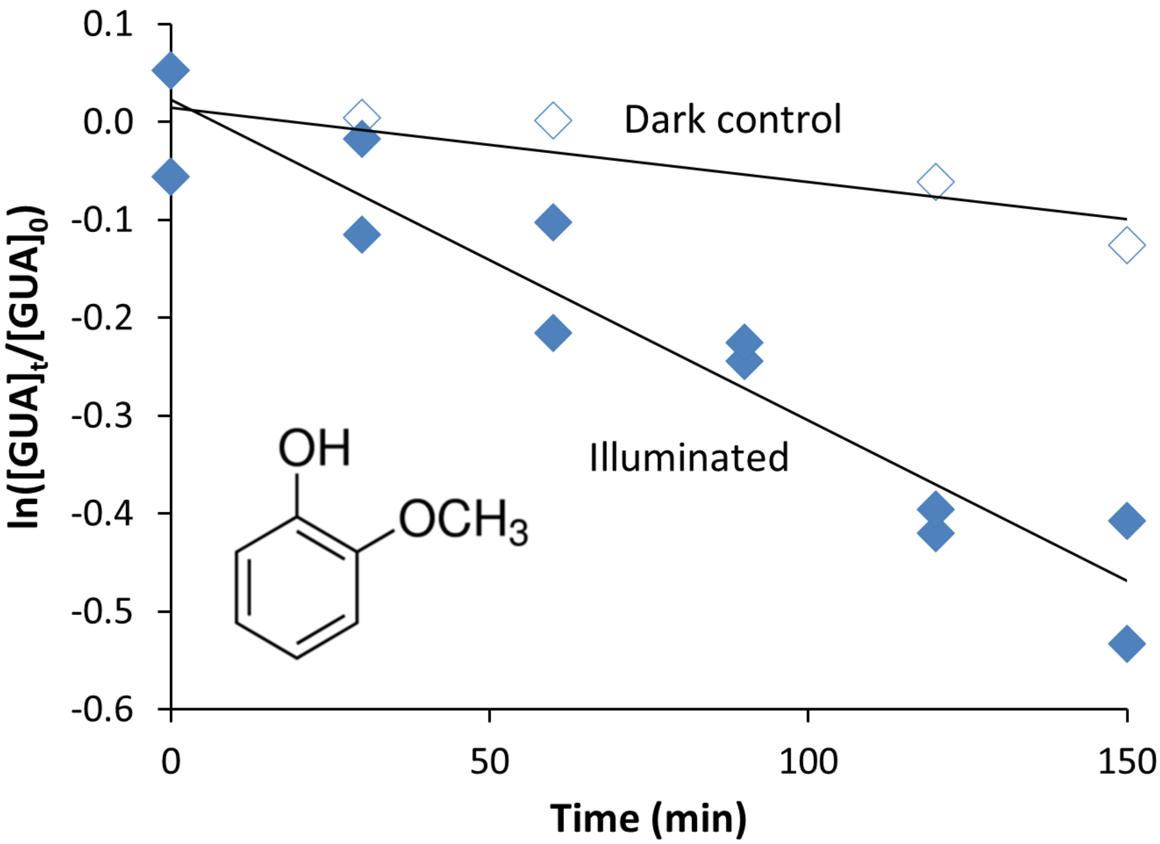


**Figure 1.** Loss of guaiacol (GUA) vapor-deposited to snow illuminated under Light Condition 1 (LC1) (blue diamonds) and in the dark (open diamonds). Each data point is from an individual sample container; there are two separate illuminated samples at each time point. The value for $j_{2NB}$ (determined in aqueous solution and converted to the equivalent value in snow) is 0.0024 $s^{-1}$ and the initial guaiacol concentration (after melting) is 3 µM.

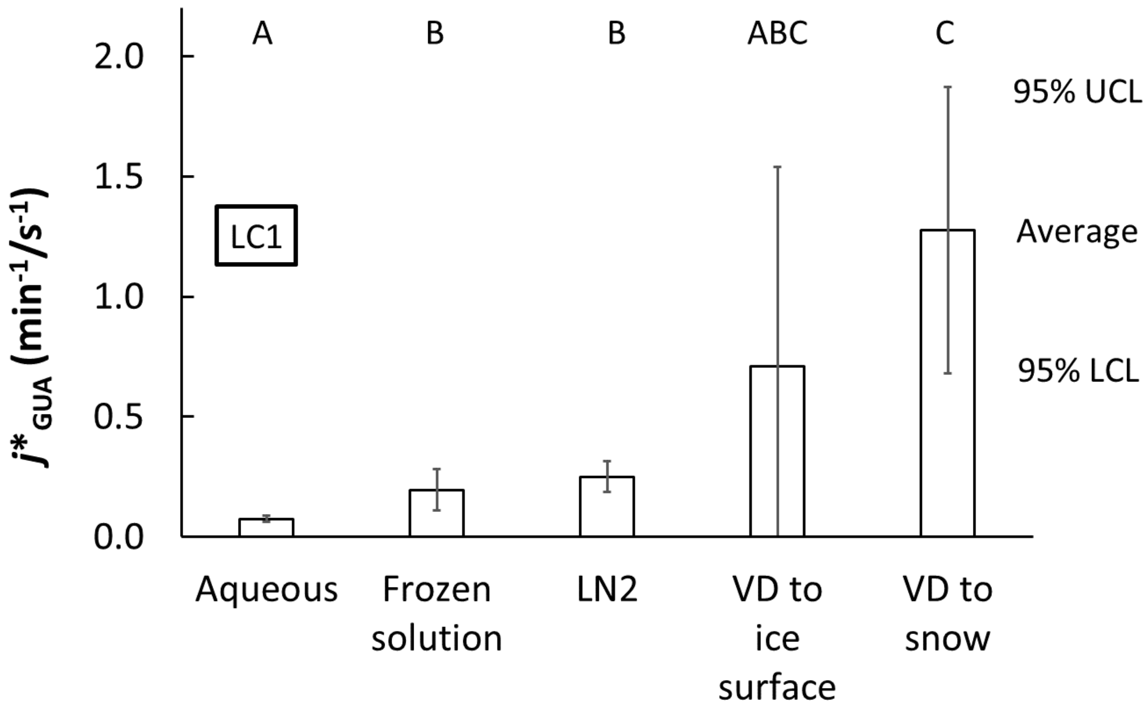


**Figure 2.** Photon-flux-normalized photodegradation rate constants for guaiacol ($j^*_{GUA}$) under LC1 conditions for each sample preparation method: aqueous solution, solution frozen in laboratory freezer, solution frozen in liquid nitrogen, vapor-deposited to a water ice surface ("VD to ice surface"), and vapor-deposited to nature-identical snow ("VD to snow"). Samples were illuminated at 5 °C (aqueous samples) or -10 °C (all others). Bars indicate the mean value for each sample preparation method (*n* = 4 - 6), with 95% upper and lower confidence limits (UCL and LCL). Sample types having statistically indistinguishable average rate constants as determined by a Tukey-Kramer test ($P < 0.05$) are labeled with the same capital letter ("A", "B", or "C"); sample types with different letters have statistically different means.

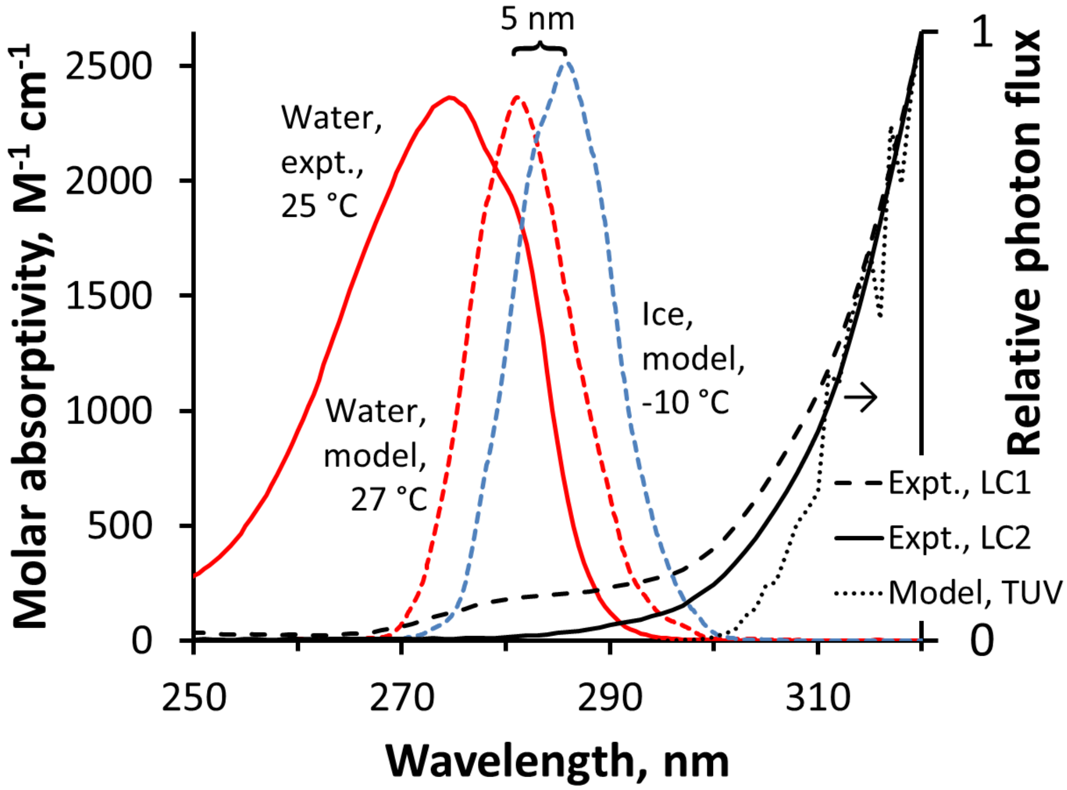


**Figure 3.** Light absorption by guaiacol along with photon fluxes in our experiments and the Arctic. Colored lines represent the measured molar absorptivities in aqueous solution (red line), modeled aqueous absorbance (red dashed) and modeled absorbance on an ice surface (blue dashed). The "5 nm" label represents the modeled bathochromic shift for absorbance on ice versus in solution. Because the absorbance values of the modeled spectra are in arbitrary units, the peak height of the modeled solution spectrum was fixed to equal the measured solution spectrum and the modeled ice spectrum was adjusted by the same factor. Black lines (right axis) show relative photon fluxes for the experimental LC1 and LC2 conditions, as well as for Summit, Greenland at midday on the summer solstice from the TUV model. Photon fluxes are relative and have been normalized to a value of unity at 320 nm.

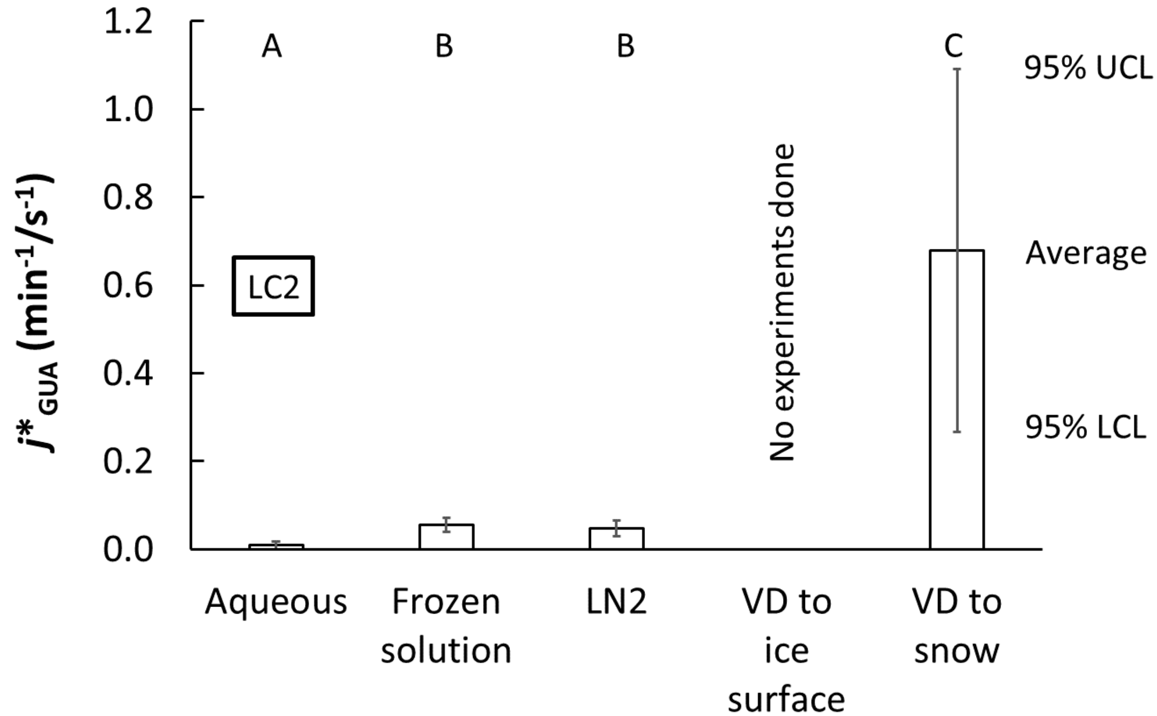


**Figure 4.** Similar to Figure 2, but for LC2 light conditions. Photon flux-normalized photodegradation rate constants for guaiacol ($j^*_{GUA}$) for four sample preparation methods; vapor-deposited to ice surface ("VD to ice surface") samples were not run for LC2. Bars indicate the mean value for each sample preparation method, with 95% upper and lower confidence limits (UCL and LCL). Sample types having statistically indistinguishable average rate constants are labeled with the same letter ("A", "B", or "C").

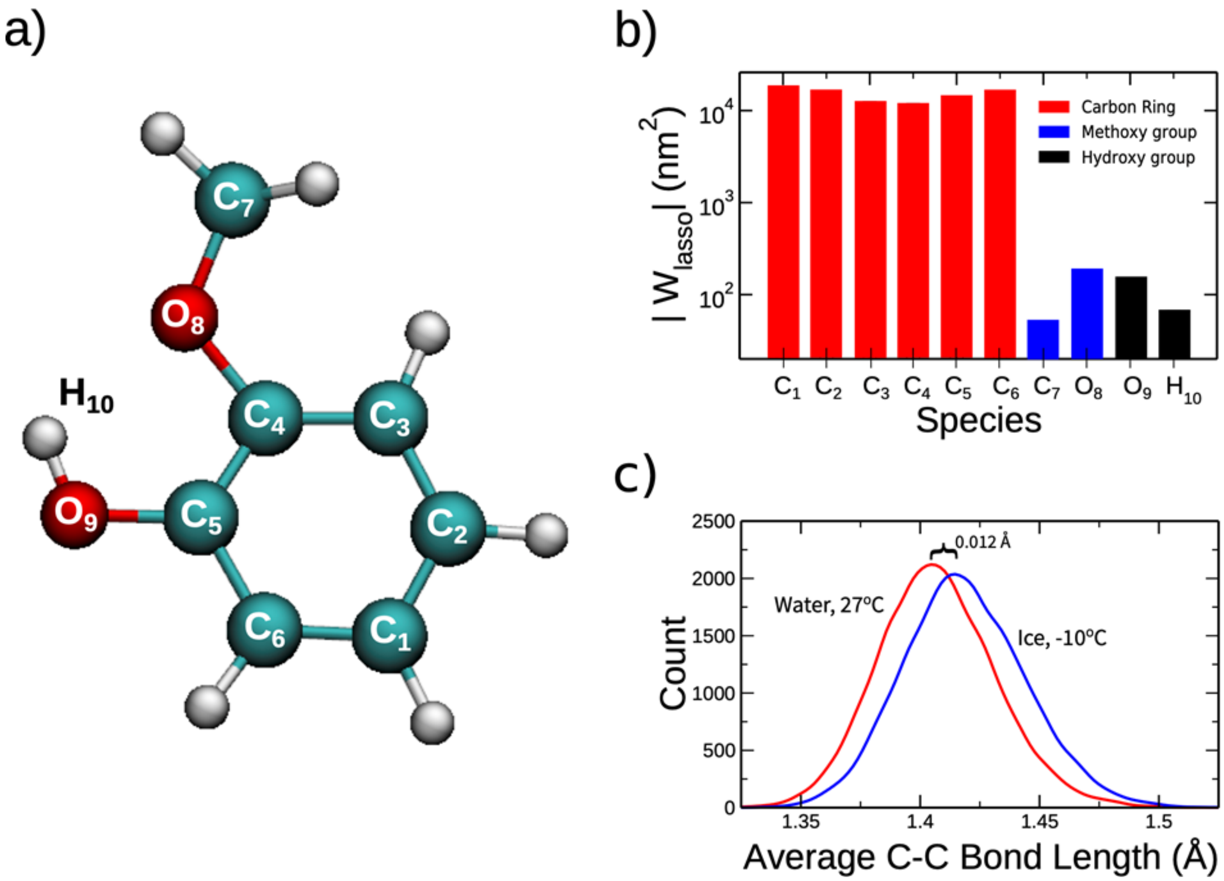


**Figure 5.** a) Diagram of guaiacol molecule, showing atom labels. b) Results of LASSO analysis showing atom-wise contribution to modeled shift in absorbance spectrum. $|W_{LASSO}|$ is the absolute magnitude of the weight parameters from the LASSO model, expressed in $nm^2$. The aromatic ring carbons are the major contributors to the computed absorbance shift. c) Distribution of computed average carbon-carbon bond lengths for the guaiacol aromatic ring in solution (27 °C) and on the ice surface (-10 °C), showing a 0.012 Å shift increase in typical bond length on the ice surface. These results indicate a considerable change in guaiacol molecular conformation between the two different environments.

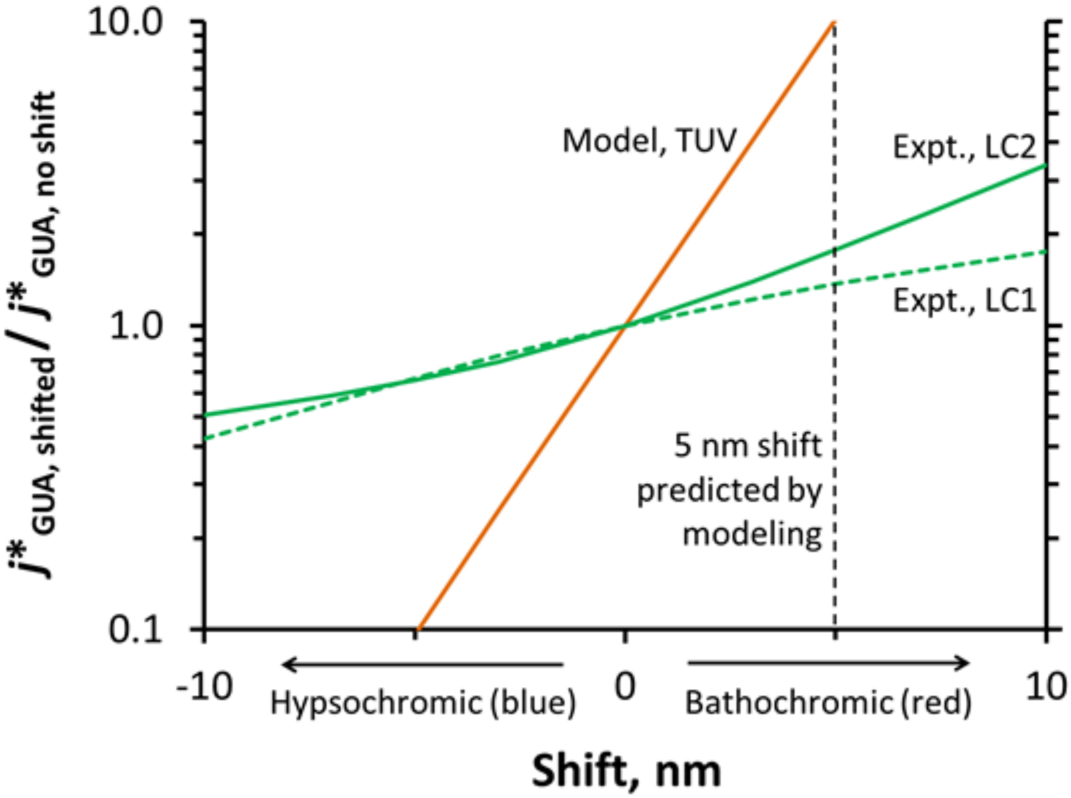


**Figure 6.** Predicted changes in $j^*_{GUA}$ values resulting from various shifts in the guaiacol light absorbance spectrum relative to the aqueous (unshifted) spectrum. Hypsochromic (blue) shifts are represented by leftward movement on the X axis, while bathochromic (red) shifts are to the right. $j^*_{GUA}$ values with a given shift were calculated using the TUV modeled actinic flux on the summer solstice for Summit, Greenland (orange line); measured flux for experimental condition LC1 (green dashed line); or measured flux for experimental condition LC2 (green solid line). The vertical dashed line shows the 5-nm bathochromic shift predicted for guaiacol by our molecular modeling.

## References


1. T. Bartels-Rausch, H. W. Jacobi, T. F. Kahan, J. L. Thomas, E. S. Thomson, J. P. D. Abbatt, M. Ammann, J. R. Blackford, H. Bluhm, C. Boxe, F. Domine, M. M. Frey, I. Gladich, M. I. Guzman, D. Heger, T. Huthwelker, P. Klan, W. F. Kuhs, M. H. Kuo, S. Maus, S. G. Moussa, V. F. McNeill, J. T. Newberg, J. B. C. Pettersson, M. Roeselova and J. R. Sodeau, A review of air-ice chemical and physical interactions (AICI): liquids, quasi-liquids, and solids in snow, *Atmos. Chem. Phys.*, 2014, **14**, 1587-1633.
2. F. Domine and P. B. Shepson, Air-snow interactions and atmospheric chemistry, *Science*, 2002, **297**, 1506-1510.
3. A. M. Grannas, A. E. Jones, J. Dibb, M. Ammann, C. Anastasio, H. J. Beine, M. Bergin, J. Bottenheim, C. S. Boxe, G. Carver, G. Chen, J. H. Crawford, F. Domine, M. M. Frey, M. I. Guzman, D. E. Heard, D. Helmig, M. R. Hoffmann, R. E. Honrath, L. G. Huey, M. Hutterli, H. W. Jacobi, P. Klan, B. Lefer, J. McConnell, J. Plane, R. Sander, J. Savarino, P. B. Shepson, W. R. Simpson, J. R. Sodeau, R. von Glasow, R. Weller, E. W. Wolff and T. Zhu, An overview of snow photochemistry: evidence, mechanisms and impacts, *Atmos. Chem. Phys.*, 2007, **7**, 4329-4373.
4. J. E. Dibb and M. Arsenault, Shouldn't snowpacks be sources of monocarboxylic acids?, *Atmos. Environ.*, 2002, **36**, 2513-2522.
5. A. L. Sumner and P. B. Shepson, Snowpack production of formaldehyde and its effect on the Arctic troposphere, *Nature*, 1999, **398**, 230-233.
6. M. Barret, F. Domine, S. Houdier, J. C. Gallet, P. Weibring, J. Walega, A. Fried and D. Richter, Formaldehyde in the Alaskan Arctic snowpack: Partitioning and physical processes involved in air-snow exchanges, *J. Geophys. Res.-Atmos.*, 2011, **116**.
7. H. W. Jacobi, R. C. Bales, R. E. Honrath, M. C. Peterson, J. E. Dibb, A. L. Swanson and M. R. Albert, Reactive trace gases measured in the interstitial air of surface snow at Summit, Greenland, *Atmos. Environ.*, 2004, **38**, 1687-1697.
8. G. J. Phillips and W. R. Simpson, Verification of snowpack radiation transfer models using actinometry, *J. Geophys. Res.-Atmos.*, 2005, **110**.
9. E. S. Galbavy, C. Anastasio, B. L. Lefer and S. R. Hall, Light penetration in the snowpack at Summit, Greenland: Part 1 Nitrite and hydrogen peroxide photolysis, *Atmos. Environ.*, 2007, **41**, 5077-5090.
10. J. L. France, M. D. King, M. M. Frey, J. Erbland, G. Picard, S. Preunkert, A. MacArthur and J. Savarino, Snow optical properties at Dome C (Concordia), Antarctica; implications for snow emissions and snow chemistry of reactive nitrogen, *Atmos. Chem. Phys.*, 2011, **11**, 9787-9801.
11. T. F. Kahan and D. J. Donaldson, Photolysis of polycyclic aromatic hydrocarbons on water and ice surfaces, *J. Phys. Chem. A.*, 2007, **111**, 1277-1285.
12. T. F. Kahan, R. Zhao, K. B. Jumaa and D. J. Donaldson, Anthracene photolysis in aqueous solution and ice: Photon flux dependence and comparison of kinetics in bulk ice and at the air-ice interface, *Environ. Sci. Technol.*, 2010, **44**, 1302-1306.
13. T. F. Kahan, N. O. A. Kwamena and D. J. Donaldson, Different photolysis kinetics at the surface of frozen freshwater vs. frozen salt solutions, *Atmos. Chem. Phys.*, 2010, **10**, 10917-10922.
14. L. Chu and C. Anastasio, Temperature and wavelength dependence of nitrite photolysis in frozen and aqueous solutions, *Environ. Sci. Technol.*, 2007, **41**, 3626-3632.

15. L. Chu and C. Anastasio, Formation of hydroxyl radical from the photolysis of frozen hydrogen peroxide, *J. Phys. Chem. A.*, 2005, **109**, 6264-6271.
16. L. Chu and C. Anastasio, Quantum yields of hydroxyl radical and nitrogen dioxide from the photolysis of nitrate on ice, *J. Phys. Chem. A.*, 2003, **107**, 9594-9602.
17. K. Ram and C. Anastasio, Photochemistry of phenanthrene, pyrene, and fluoranthene in ice and snow, *Atmos. Environ.*, 2009, **43**, 2252-2259.
18. T. Hullar, D. Magadia and C. Anastasio, Photodegradation Rate Constants for Anthracene and Pyrene Are Similar in/on Ice and in Aqueous Solution, *Environ. Sci. Technol.*, 2018, **52**, 12225-12234.
19. E. S. Galbavy, C. Anastasio, B. Lefer and S. Hall, Light penetration in the snowpack at Summit, Greenland: Part 2 Nitrate photolysis, *Atmos. Environ.*, 2007, **41**, 5091-5100.
20. E. S. Galbavy, K. Ram and C. Anastasio, 2-Nitrobenzaldehyde as a chemical actinometer for solution and ice photochemistry, *J. Photochem. Photobiol. A-Chem.*, 2010, **209**, 186-192.
21. A. S. McFall and C. Anastasio, Photon flux dependence on solute environment in water ices, *Environmental Chemistry*, 2016, **13**, 682-687.
22. C. Z. Zhu, B. Xiang, L. T. Chu and L. Zhu, 308 nm Photolysis of Nitric Acid in the Gas Phase, on Aluminum Surfaces, and on Ice Films, *J. Phys. Chem. A.*, 2010, **114**, 2561-2568.
23. A. S. McFall, K. C. Edwards and C. Anastasio, Nitrate Photochemistry at the Air-Ice Interface and in Other Ice Reservoirs, *Environ. Sci. Technol.*, 2018, **52**, 5710-5717.
24. T. F. Kahan and D. J. Donaldson, Benzene photolysis on ice: Implications for the fate of organic contaminants in the winter, *Environ. Sci. Technol.*, 2010, **44**, 3819-3824.
25. R. Kania, J. K. Malongwe, D. Nachtigallová, J. Krausko, I. Gladich, M. Roeselová, D. Heger and P. Klán, Spectroscopic properties of benzene at the air-ice interface: A combined experimental-computational approach, *J. Phys. Chem. A.*, 2014, **118**, 7535-7547.
26. N. Matykiewiczová, R. Kurkova, J. Klanova and P. Klán, Photochemically induced nitration and hydroxylation of organic aromatic compounds in the presence of nitrate or nitrite in ice, *J. Photochem. Photobiol. A-Chem.*, 2007, **187**, 24-32.
27. D. Heger, J. Jirkovsky and P. Klán, Aggregation of methylene blue in frozen aqueous solutions studied by absorption spectroscopy, *J. Phys. Chem. A.*, 2005, **109**, 6702-6709.
28. J. Krausko, J. K. Malongwe, G. Bičanová, P. Klán, D. Nachtigallová and D. Heger, Spectroscopic properties of naphthalene on the surface of ice grains revisited: A combined experimental computational approach, *J. Phys. Chem. A.*, 2015, **119**, 8565-8578.
29. J. K. Malongwe, D. Nachtigallová, P. Corrochano and P. Klán, Spectroscopic properties of anisole at the air-ice interface: A combined experimental-computational approach, *Langmuir*, 2016, **32**, 5755-5764.
30. P. Corrochano, D. Nachtigallová and P. Klán, Photooxidation of Aniline Derivatives Can Be Activated by Freezing Their Aqueous Solutions, *Environ. Sci. Technol.*, 2017, **51**, 13763-13770.
31. S. Gopalakrishnan, P. Jungwirth, D. J. Tobias and H. C. Allen, Air-Liquid Interfaces of Aqueous Solutions Containing Ammonium and Sulfate: Spectroscopic and Molecular Dynamics Studies, *J. Phys. Chem. B*, 2005, **109**, 8861–8872.

32. P. Jungwirth and D. J. Tobias, Specific Ion Effects at the Air/Water Interface, *Chem. Rev.*, 2006, **106**, 1259–1281.

33. R. Vácha, L. Cwiklik, J. Řezáč, P. Hobza, P. Jungwirth, K. Valsaraj, S. Bahr and V. Kempter, Adsorption of Aromatic Hydrocarbons and Ozone at Environmental Aqueous Surfaces *J. Phys. Chem. A* 2008, **112**, 4942–4950.

34. R. B. Gerber, M. E. Varner, A. D. Hammerich, S. Riikonen, G. Murdachaew, D. Shemesh and B. J. Finlayson-Pitts, Computational Studies of Atmospherically-Relevant Chemical Reactions in Water Clusters and on Liquid Water and Ice Surfaces, *Accounts Chem. Res.*, 2015, **48**, 399-406.

35. D. Heger, D. Nachtigallová, F. Surman, J. Krausko, B. Magyarova, M. Brumovsky, M. Rubes, I. Gladich and P. Klán, Self-Organization of 1-Methylnaphthalene on the Surface of Artificial Snow Grains: A Combined Experimental-Computational Approach, *J. Phys. Chem. A.*, 2011, **115**, 11412-11422.

36. R. Kurkova, D. Ray, D. Nachtigallová and P. Klán, Chemistry of small organic molecules on snow grains: The applicability of artificial snow for environmental studies, *Environ. Sci. Technol.*, 2011, **45**, 3430-3436.

37. H. W. Jacobi, T. Annor and E. Quansah, Investigation of the photochemical decomposition of nitrate, hydrogen peroxide, and formaldehyde in artificial snow, *J. Photochem. Photobiol. A-Chem.*, 2006, **179**, 330-338.

38. S. Schleef, M. Jaggi, H. Lowe and M. Schneebeli, An improved machine to produce nature-identical snow in the laboratory, *J. Glaciol.*, 2014, **60**, 94-102.

39. J. J. Schauer, M. J. Kleeman, G. R. Cass and B. R. T. Simoneit, Measurement of emissions from air pollution sources. 3. C-1-C-29 organic compounds from fireplace combustion of wood, *Environ. Sci. Technol.*, 2001, **35**, 1716-1728.

40. I. Timrov, M. Micciarelli, M. Rosa, A. Calzolari and S. Baroni, Multimodel Approach to the Optical Properties of Molecular Dyes in Solution, *J. Chem. Theory Comput.*, 2016, **12**, 4423-4429.

41. J. Bones and E. Adams, Davos, Switzerland, 2009.

42. H. Nakamura, A new apparatus to produce fresh snow, *Rep. Natl Res. Cent. Disaster Prev.*, 1978, **19**, 229-237.

43. M. A. Sanchez, T. Kling, T. Ishiyama, M. J. van Zadel, P. J. Bisson, M. Mezger, M. N. Jochum, J. D. Cyran, W. J. Smit, H. J. Bakker, M. J. Shultz, A. Morita, D. Donadio, Y. Nagata, M. Bonn and E. H. G. Backus, Experimental and theoretical evidence for bilayer-by-bilayer surface melting of crystalline ice, *Proc. Natl. Acad. Sci. U. S. A.*, 2017, **114**, 227-232.

44. T. Kling, F. Kling and D. Donadio, Structure and Dynamics of the Quasi-Liquid Layer at the Surface of Ice from Molecular Simulations, *J. Phys. Chem. C*, 2018, **122**, 24780-24787.

45. M. E. Casida, H. Chermette and D. Jacquemin, Time-dependent density-functional theory for molecules and molecular solids Preface, *Theochem-J. Mol. Struct.*, 2009, **914**, 1-2.

46. D. Rocca, R. Gebauer, Y. Saad and S. Baroni, Turbo charging time-dependent density-functional theory with Lanczos chains, *J. Chem. Phys.*, 2008, **128**, 14.

47. O. Andreussi, I. Dabo and N. Marzari, Revised self-consistent continuum solvation in electronic-structure calculations, *J. Chem. Phys.*, 2012, **136**, 20.

48. O. Andreussi and N. Marzari, Electrostatics of solvated systems in periodic boundary conditions, *Phys. Rev. B*, 2014, **90**, 16.

49. X. C. Ge, I. Timrov, S. Binnie, A. Biancardi, A. Calzolari and S. Baroni, Accurate and Inexpensive Prediction of the Color Optical Properties of Anthocyanins in Solution, *J. Phys. Chem. A.*, 2015, **119**, 3816-3822.
50. R. Tibshirani, Regression shrinkage and selection via the lasso: a retrospective, *J. R. Stat. Soc. Ser. B-Stat. Methodol.*, 2011, **73**, 273-282.
51. F. Bononi, Bathochromic shift in the UV-Visible Absorption Spectra of Phenols at Ice Surfaces: Insights from First-Principles Calculations, *In preparation*, 2020.
52. J. D. Smith, V. Sio, L. Yu, Q. Zhang and C. Anastasio, Secondary Organic Aerosol Production from Aqueous Reactions of Atmospheric Phenols with an Organic Triplet Excited State, *Environ. Sci. Technol.*, 2014, **48**, 1049-1057.
53. Z. Y. Chen and C. Anastasio, Concentrations of a triplet excited state are enhanced in illuminated ice, *Environ. Sci.-Process Impacts*, 2017, **19**, 12-21.
54. M. Parac and S. Grimme, A TDDFT study of the lowest excitation energies of polycyclic aromatic hydrocarbons, *Chem. Phys.*, 2003, **292**, 11-21.
55. S. Madronich and S. J. Flocke, in *Handbook of Environmental Chemistry*, ed. P. Boule, Springer, Heidelberg, 1998, pp. 1-26.
56. J. R. McConnell, R. Edwards, G. L. Kok, M. G. Flanner, C. S. Zender, E. S. Saltzman, J. R. Banta, D. R. Pasteris, M. M. Carter and J. D. W. Kahl, 20th-century industrial black carbon emissions altered arctic climate forcing, *Science*, 2007, **317**, 1381-1384.
57. A. Pokhrel, K. Kawamura, B. Kunwar, K. Ono, A. Tsushima, O. Seki, S. Matoba and T. Shiraiwa, Ice core records of levoglucosan and dehydroabietic and vanillic acids from Aurora Peak in Alaska since the 1660s: a proxy signal of biomass-burning activities in the North Pacific Rim, *Atmos. Chem. Phys.*, 2020, **20**, 597-612.
58. X. Wan, K. Kawamura, K. Ram, S. C. Kang, M. Loewen, S. P. Gao, G. M. Wu, P. Q. Fu, Y. L. Zhang, H. Bhattarai and Z. Y. Cong, Aromatic acids as biomass-burning tracers in atmospheric aerosols and ice cores: A review, *Environ. Pollut.*, 2019, **247**, 216-228.
59. G. T. Shi, X. C. Wang, Y. S. Li, R. Trengove, Z. Y. Hu, M. Mi, X. C. Li, J. H. Yu, B. Hunter and T. H. He, Organic tracers from biomass burning in snow from the coast to the ice sheet summit of East Antarctica, *Atmos. Environ.*, 2019, **201**, 231-241.
60. Z. Y. Chen, L. Chu, E. S. Galbavy, K. Ram and C. Anastasio, Hydroxyl radical in/on illuminated polar snow: formation rates, lifetimes, and steady-state concentrations, *Atmos. Chem. Phys.*, 2016, **16**, 9579-9590.
61. J. D. Smith, H. Kinney and C. Anastasio, Aqueous benzene-diols react with an organic triplet excited state and hydroxyl radical to form secondary organic aerosol, *Phys. Chem. Chem. Phys.*, 2015, **17**, 10227-10237.